Real Time Needle Tracking with NeedleGAN:

A CGAN and Mask-RCNN based Architecture for Automatic Generation, Segmentation, and Localization of Physical Needles for MR-guided Percutaneous Hepatic Interventions

Gopalaniruddh S. Tadinada[1, 2], Junichi Tokuda[2]

DuPont Manual High School, 120 W Lee St, Louisville, KY 40208[1]

Harvard Medical School and Brigham and Women's Hospital, Boston, MA 02215[2]

Background

Liver Cancer can be detrimental to major digestive organs and result in life threatening conditions. In this past year, Liver Cancer saw an increase of 900,000 cases and 830,000 deaths worldwide (2). The surrounding hepatic portal vein system and lymph nodes make the spread of cancerous cells to multiple organs much easier resulting in a 5 year survival rate of just 18% (3), making it one of the most deadly diseases today.

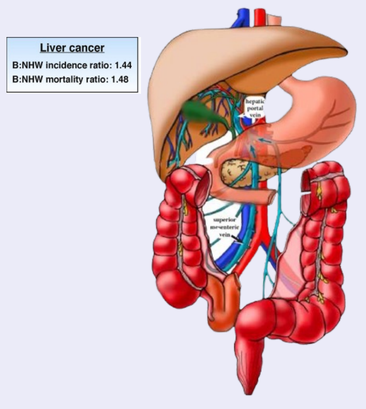

Figure 1 (Left): Visualization of the digestive tract & organs, as well as the HPVS and Lymphatic vessels in close proximity, with Liver cancer having a high incidence rate. Source: *(Ashktorab 2017)*

The current definitive confirmatory test for liver cancer is a percutaneous liver biopsy, where a small needle is inserted through the stomach and into the liver in order to remove a small portion of the tissue for analysis. In most cases this biopsy is guided by ultrasound and randomly samples small sections of the liver, resulting in the test missing aggressive tumors. In fact, the false negative rate of US-guided percutaneous liver biopsies reaches 30%.

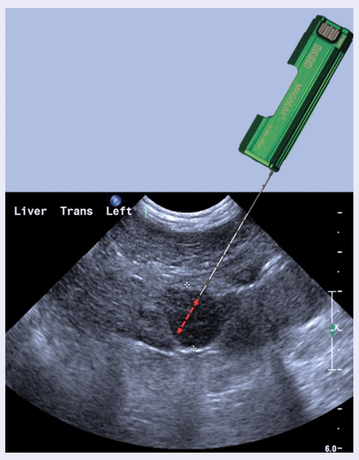

Figure 2: Ultrasound Guided Percutaneous Liver Biopsy Source: (Kumar 2019)

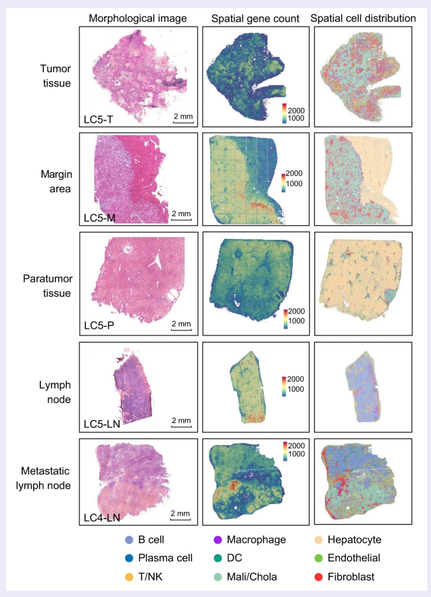

Figure 3: Representation of different levels of liver cancer, the rapid progression, and aggressive behavior. Source: (Armaghany 2012)

MR-Guided Percutaneous Liver Biopsy

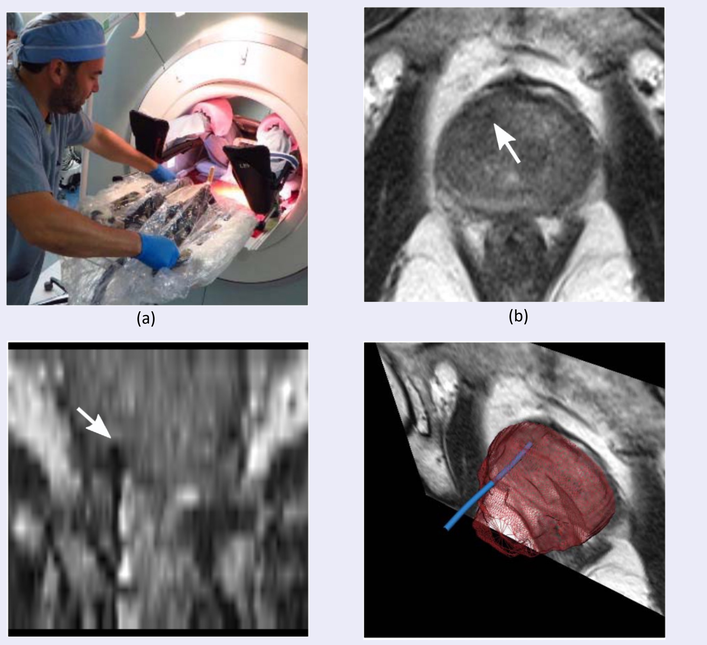

Figure 4: (a) The patient is placed in the supine position in the MRI gantry, and his legs are elevated to allow for transperineal access. The skin of the perineum is prepared and draped in a sterile manner, and the needle guidance template is positioned. **(b) and (c)** Axial and coronal views of intraprocedural T2-W MRI with needle tip marked by white arrow. **(d)** 3D rendering of the needle (blue), segmented by my method, and visualized relative to the liver, and an MRI cross-section that is orthogonal to the plane containing the needle tip.

MRI has actually demonstrated value in improving guided liver biopsies as MRI can identify suspicious masses, thus requiring less cores of tissue, and revealing a significantly higher ratio of cancer involvement to tissue core. Advances in real-time MRI also allow physicians to check the placement and trajectory of the needle compared to the location of the suspicious mass, and make adjustments accordingly.

Real time tracking of the needle poses a few challenges. Parts of a needle under the MRI appear different from scan to scan, and is also difficult to distinguish from nearby tissue as can be seen in this image. Secondly, due to the substantially different magnetic resonance properties of the inserted needle and surrounding tissue, a loss of signal is apparent around the needle which is known as the needle artifact. According to studies, the discrepancy of the true needle position from the artifact can extend 9mm longitudinally, and display extreme curvature in the direction of B0 magnetic field. The size of early stage liver lesions is <20 millimeters, which means that in many cases it is unknown as to whether the needle hit the lesion or not.

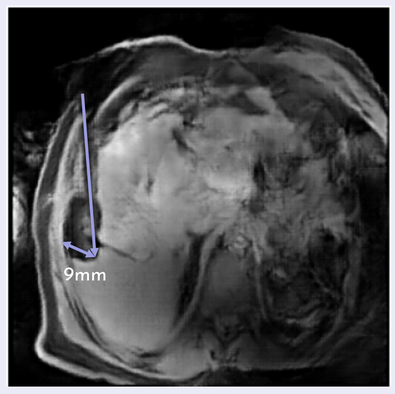

Figure 5: Needle Artifact from intraoperative MRI scan of percutaneous liver biopsy.

Engineering Goals

- Generate a synthetic dataset that can accurately recreate single slice MR induced needle artifacts
- Create an algorithm to automatically localize the position of the artifact and distinguish it from surrounding tissue
- Create a client-side web application that facilitates easy device usage and connection to the screening model

Synthetic Data Generation - CGAN

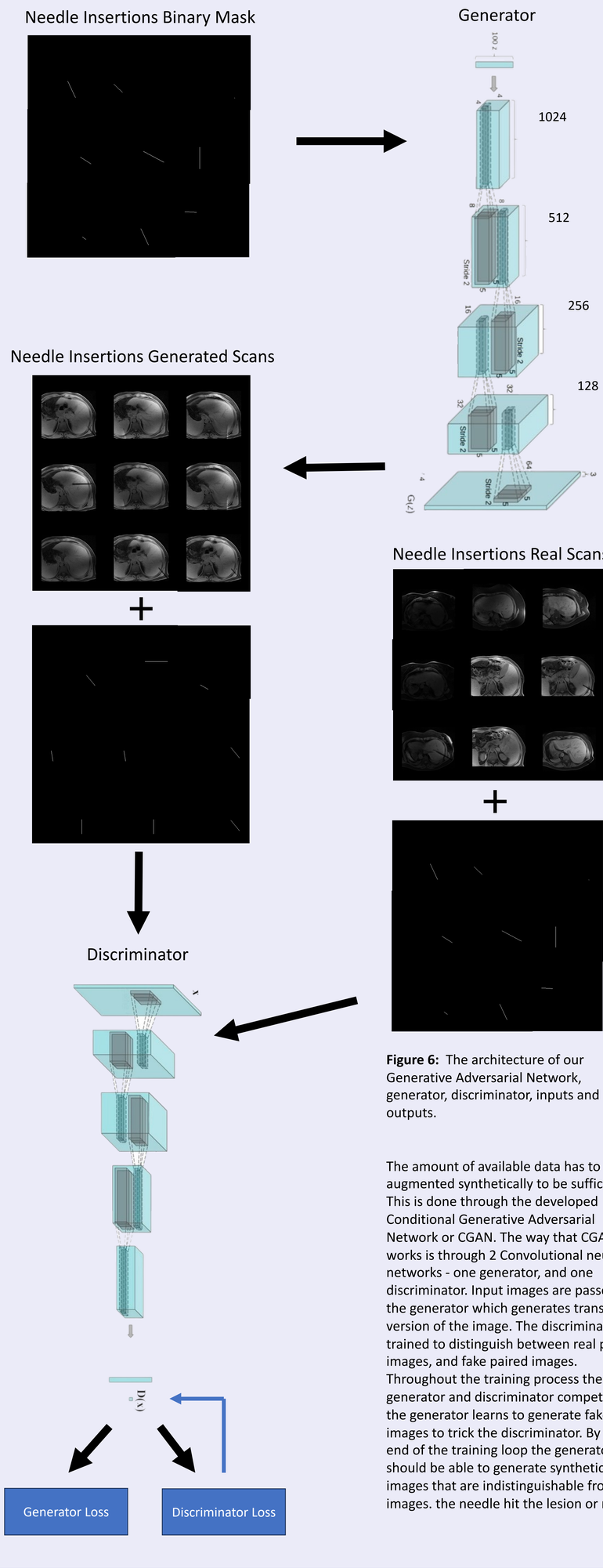

Figure 6: The architecture of our Generative Adversarial Network, generator, discriminator, inputs and outputs.

The amount of available data has to be augmented synthetically to be sufficient. This is done through the developed Conditional Generative Adversarial Network or CGAN. The way that CGAN works is through 2 Convolutional neural networks - one generator, and one discriminator. Input images are passed into the generator which generates translated version of the image. The discriminator is trained to distinguish between real paired images, and fake paired images. Throughout the training process the generator and discriminator compete as the generator learns to generate fake images to trick the discriminator. By the end of the training loop the generator should be able to generate synthetic images that are indistinguishable from real images. the needle hit the lesion or not.

Synthetic Data Generation Results

Figure 7: Visualizing the losses of the generator (light blue) and discriminator (dark blue) throughout the training process as the epochs increase. The generator loss increased during the beginning of the training loop until the 50th epoch, after which it significantly decreased, which signifies that it started learning the distribution of data in the images at the 50th epoch. The discriminator and generator loss should be contrasting meaning that when the generator loss goes up/down, the discriminator loss should go down/up respectively.

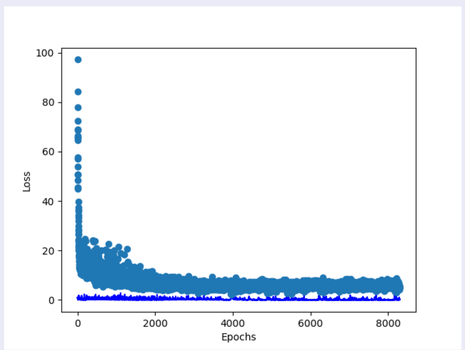

Figure 8: Visualizing the images generated by the GAN at the end of the training loop. The 3 images in the top row are binary masks passed into the GAN. The images in the middle row are generated by the GAN. The images in the last row are the ground truth images which are paired to the ground truth binary masks. Upon visual inspection the generated images look perfectly alike to the ground truth images. This is supported by the SSIM (structural similarity index) of the generated training dataset against the original dataset preserved for validation, since it is 0.944 average with a 0.02 standard deviation.

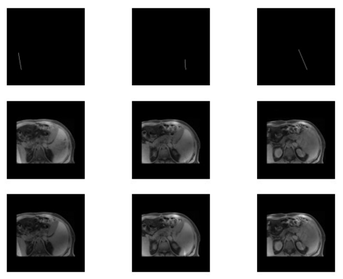

Needle Localization – Mask RCNN

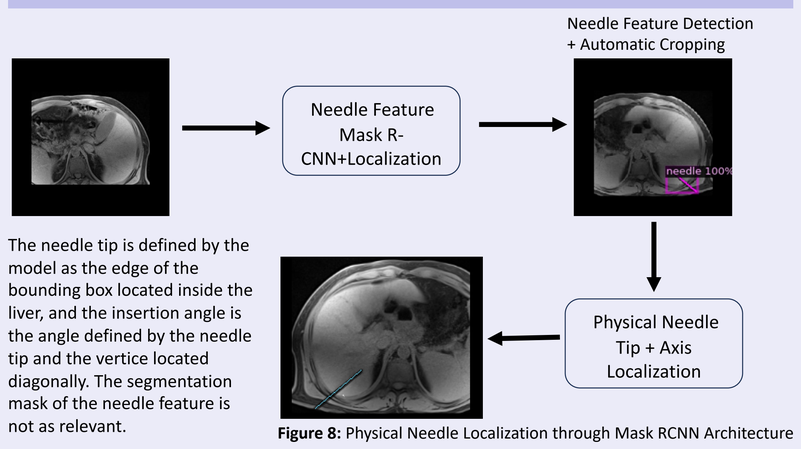

The needle tip is defined by the model as the edge of the bounding box located inside the liver, and the insertion angle is the angle defined by the needle tip and the vertice located diagonally. The segmentation mask of the needle feature is not as relevant.

Figure 8: Physical Needle Localization through Mask RCNN Architecture

Validation Dataset Preparation

Figure 9: Preparing the Validation Dataset by acquiring needle artifacts at various angles.

Needle Localization Results

dxy	0	10	20	30	40	50	60	70	80	90
Mean	0.960485077	1.720938676	1.07298848	0.732430495	0.732444438	1.295879564	1.929349725	1.35629876	1.242935079	0.658892452
SD	0.257841106	0.128542209	0.09556382	0.232209346	0.195622407	0.350076533	0.324222092	0.25120663	0.135880362	0.173369315
Max	1.674722002	2.360238544	1.45902335	1.056982376	0.890452548	1.960346128	2.479238544	1.82445096	1.539604014	0.925679552

Table 1: Table for needle tip localization results. dxy represents the Euclidean distance between the predicted needle tip and the true needle tip. Mean, Standard Deviation, and maximum difference for dxy are listed for each angle.

dΘ	0	10	20	30	40	50	60	70	80	90
Mean	-0.2967234	-1.04109891	-0.122675	0.946445713	0.031685109	-0.870016328	0.577980691	-0.5093571	-0.730241232	-0.53733076
SD	0.0752166	0.22748744	0.066409	0.35375871	0.055306544	0.295996467	0.128773519	0.3224709	-0.225831052	-0.23198311
Max	1.0433562	1.84205615	0.430556	1.50437455	0.304280834	1.538600844	1.125609037	1.1925506	1.084509442	0.98022739

Table 2: Table for needle axis localization results. dΘ represents the angle between the predicted needle mask and the true needle axis. Mean, Standard Deviation, and maximum difference for dΘ are listed for each angle.

Success Rate	0	10	20	30	40	50	60	70	80	90
dxy<1.37mm or dΘ<1	0.97	0.75	1	0.83	1	0.77	0.88	0.87	0.92	1

Table 3: Table for needle localization success rate. Success rate is defined as the Euclidean distance between the predicted needle tip and true needle tip being less than 1.37mm (1 pixel), or the difference between the predicted needle axis and true needle axis being less than 1°.

Conclusions

- Tuning the GAN to focus on generating needle artifacts in anatomically correct positions, instead of randomly, in order to avoid scans where needles are going through other organs for example, kidneys or the spine
- I would also look to train my model to determine the slice that contains the needle tip in it, in order make my single slice model more accurate
- I would also look to generate volumetric data in order to create a model that can determine true needle position without assuming the needle is perfectly aligned with the MRI scan plane
- Lastly, I hope to implement this tracking algorithm as an extension in 3D Slicer so that it can be tested during real patient interventions

Acknowledgements

Acknowledgments:

I would like to give my sincere thanks to Dr. Junichi Tokuda and Mariana Bernarderes from the Surgical Planning Laboratory, part of the National Center for Image Guided Therapy, Harvard Medical School and Brigham and Women's Hospital, for providing me with resources over the last 6 weeks to conduct this project. I would also like to thank the RISE program for giving me this opportunity.

References

References:

1. Li, Xinzhou, et al. "Physics-Driven Mask R-CNN for Physical Needle Localization in MRI-Guided Percutaneous Interventions." *IEEE Access*, vol. 9, 2021, pp. 161055–161068, https://doi.org/10.1109/access.2021.3128163.
2. Liu, Yao, and Lianxin Liu. "Changes in the Epidemiology of Hepatocellular Carcinoma in Asia." *Cancers*, 15 Sept. 2022, www.ncbi.nlm.nih.gov/pmc/articles/PMC9496757/.
3. "Liver Cancer Survival Rates: Cancer of the Liver Survival Rates." *Cancer of the Liver Survival Rates | American Cancer Society*, www.cancer.org/cancer/types/liver-cancer/detection-diagnosis-staging/survival-rates.html. Accessed 7 Aug. 2023.
4. "Liver Cancer." *Mayo Clinic*, 28 Apr. 2023, www.mayoclinic.org/diseases-conditions/liver-cancer/symptoms-causes/syc-20353659.
5. Mehrtash, Alireza, et al. "Automatic Needle Segmentation and Localization in MRI with 3-D Convolutional Neural Networks: Application to MRI-Targeted Prostate Biopsy." *IEEE Transactions on Medical Imaging*, vol. 38, no. 4, 2019, pp. 1026–1036, https://doi.org/10.1109/tmi.2018.2876796.
6. Vernuccio, Federica, et al. "Negative Biopsy of Focal Hepatic Lesions: Decision Tree Model for Patient Management." *American Journal of Roentgenology*, vol. 212, no. 3, 2019, pp. 677–685, https://doi.org/10.2214/ajr.18.20268.